Wind and Structures, *Vol. 29, No. 1 (2019) 33-41*
DOI: https://doi.org/10.12989/was.2019.29.1.033

Diffraction of water waves by an array of vertical barriers and heterogeneous bottom

R. Mondal[1a] and Md. Mahbub Alam[*1,2]

[1]*Institute for Turbulence-Noise-Vibration Interaction and Control*
Harbin Institute of Technology (Shenzhen), Shenzhen 518055, China
[2]*Digital Engineering Laboratory of Offshore Equipment, Shenzhen, China*

(Received September 7, 2018, Revised February 26, 2019, Accepted February 28, 2019)

Abstract. The interaction of head waves with an infinite row of identical, equally spaced, rectangular breakwaters is investigated in the presence of uneven bottom topography. Using linear water wave theory and matched eigenfunction expansion method, the boundary value problem is transformed into a system of linear algebraic equations which are numerically solved to know the velocity potentials completely. Utilizing this method, reflected and transmitted wave energy are computed for different physical parameters along with the wave field in the vicinity of breakwaters. It is observed that the wave field becomes more complicated when the incoming wavelength becomes smaller than the channel width. A critical ratio of the gap width to the channel width, corresponding to the inflection point of the transmitted energy variation, is identified for which 1/3 of the total energy is transmitted. Similarly, depending on the incident wavelength, there is a critical breakwater width for which a minimum energy is transmitted. Further, the accuracy of the computed results is verified by using the derived energy relation.

Keywords: uneven bottom; breakwaters; eigenfunction expansion

1. Introduction

Protection of coastlines, harbors and marinas from incoming ocean waves is one of the major issues in the field of coastal and port engineering. For wave attenuation, many authors (Dalrymple and Martin 1990, Williams and Crull 1993, Abul-Azam and Williams 1997, Porter and Evans 1996) proposed an array (appearing periodically) of identical screen type breakwaters parallel to the coastline. This class of problem has also received a considerable attention in the field of acoustics (Miles 1982, Achenbach and Li 1986, Linton and Evans 1993). Instead of screen type breakwaters, Fernyhough and Evans (1995) suggested an array of block type breakwaters arranged periodically. These kinds of breakwaters are environment-friendly and ecological as the gaps between two successive breakwaters allow the exchange of water, sediment and marine lives between sea and shore sides. Furthermore, Mondal *et al.* (2017) considered the problem of water wave scattering by an array of identical ports and an infinitely long floating breakwater. They evaluated the resonance frequency for different geometrical configurations. This class of problem is interesting as the waves undergo reflection, transmission, diffraction and shoaling when water waves encounter the entrance of gaps.

Apart from the wave scattering by periodic breakwaters, wave diffraction through a narrow breakwater gap was studied by Buchwald (1971) and Sobey and Johnson (1986). Oblique wave propagation through a narrow opening between two semi-infinite breakwaters was studied by Dalrymple *et al.* (2000) using two mathematical approaches: Fourier transform and buffer domain method. From their numerical computation, they observed that the wave pattern in the channel varies significantly with the angle of incident waves. Kanoria *et al.* (1999) used multi-term Galerkin approximations to compute the reflection and transmission coefficients when water waves propagate around a thick vertical barrier of rectangular cross section. They observed that the thickness of the barrier plays a significant role in the modeling of breakwaters.

The above-mentioned studies dealt with the problems having a uniform water depth while the breakwaters are constructed near the coastal region where water depth is not uniform. The problem of wave scattering by a thin finite floating dock and a step bottom was studied by Dhillon *et al.* (2016). They considered two cases such that the incident wave propagates from the lower depth as well as from the higher depth. Furthermore, Mondal and Takagi (2019) studied the wave interaction with a fixed submerged body in the presence of a step bottom in both infinite and semi-infinite fluid domains. In their study, the wave forces on the submerged body and vertical wall were computed. In addition, reflection and transmission coefficients were presented to show the effect of the submerged body on wave energy propagation. Recently, Mondal and Alam (2018) considered the problem of water wave scattering by an array of breakwaters in the presence of a step bottom in the cases of infinite and semi-infinite fluid domains. In their

[*]Corresponding author, Professor
E-mail: alamm28@yahoo.com; alam@hit.edu.cn
[a] Ph.D.
E-mail: ramju08@yahoo.com

ISSN: 1226-6116 (Print), 1598-6225 (Online)

study, the velocity potentials were computed explicitly using the eigenfunction expansion method and numerical results were presented for reflected and transmitted wave energy in the case of the infinite fluid domain for different physical parameters. However, in the case of the semi-infinite fluid domain, resonance frequency and resonance surface modes were executed. On the other hand, Newman (1965) studied the wave reflection and transmission theoretically and numerically when water waves propagate over a step bottom where the deeper region is of infinite depth. Furthermore, considering finite and semi-infinite steps, Karmakar and Sahoo (2008) investigated the scattering of water waves by a floating membrane. Bhattacharjee *et al.* (2008) analyzed the transformation of flexural gravity waves considering a change in water depth and structural characteristics. They emphasized computing the reflection and transmission coefficients and the deflection of a non-homogenous floating ice sheet.

Concrete flushing culverts, having abrupt change in water depth on either side of opening, commonly feature harbors (see Tsoukala and Moutzouris 2009, Belibassakis *et al.* 2014). The flushing culverts enhance the circulation of water by amplifying the velocity field in the harbor which maintains the water quality and biological process. The flushing culverts also harbor an harbor by reducing the transport of sediment. Furthermore, it is observed that flushing culverts are often constructed between two breakwaters as it is cost effective.

Therefore, in the present study, the work of Mondal and Alam (2018) is extended by considering embedded flushing culverts between two consecutive breakwaters. Due to the presence of culverts, the water depths in the ocean side and lee side of breakwaters, and across the gap of breakwaters are different. Hence, it is required to reformulate Mondal and Alam's (2018) problem.

2. Mathematical formulation and solution

In the present study, the linear water wave theory is used to understand the behavior of waves in the vicinity of an opening of identical rectangular breakwaters, which are extended throughout the water depth, in the presence of uneven bottom topography. The three-dimensional Cartesian coordinate system is used, with the origin at the mean free surface and the z-axis is positive in the vertically upward direction. It is assumed that the breakwaters of a width $2d$ are placed parallel to the coastline and are symmetric about the y-axis (see Fig. 1(a)). The water depths in the ocean and lee sides of breakwaters are $h^{(1)}$ and $h^{(3)}$, respectively. The gap length between two consecutive breakwaters is 2α and the water depth throughout the gap is $h^{(2)}$. Due to the periodicity of breakwaters, the present problem can be reduced to a channel problem of channel width 2β such that there is no flow across channel walls (see Mondal *et al.* 2017). Fig. 1(b) shows the top view of the channel problem. Considering the change in the channel width and water depth, the flow domain inside the channel is decomposed into three domains which are labeled with $R^{(j)}$, j=1,2, and 3, where $R^{(1)}$: $d \le x < \infty$, $-\beta \le y \le \beta$, $-h^{(1)} \le z \le \eta$; $R^{(2)}$: $-d \le x \le d$, $-\alpha \le y \le \alpha$, $-h^{(2)} \le z \le \eta$; and $R^{(3)}$: $-\infty < x \le -d$, $-\beta \le y \le \beta$, $-h^{(3)} \le z \le \eta$, where η is the free surface displacement. The bottom surface, breakwater surface and channel wall are denoted by S_b, S_{bw} and S_{cw}, respectively and defined by $S_b = (d \le x < \infty, -\beta \le y \le \beta, z = -h^{(1)}) \cup (x = d, -\beta \le y \le \beta, -h^{(1)} \le z \le -h^{(2)}) \cup (-d \le x \le d, -\alpha \le y \le \alpha, z = -h^{(2)}) \cup (x = -d, -\beta \le y \le \beta, -h^{(3)} < z < -h^{(2)}) \cup (-\infty < x \le -d, -\beta \le y \le \beta, z = -h^{(3)})$; $S_{bw} = (-\beta \le y \le -\alpha, -h^{(2)} \le z \le 0, x = \pm d) \cup (\alpha \le y \le \beta, -h^{(2)} \le z \le 0, x = \pm d) \cup (-d \le x \le d, -h^{(2)} < z < 0, y = \pm\alpha)$ and $S_{cw} = (x > d, -h^{(1)} \le z \le 0, y = \pm\beta) \cup (x < -d, -h^{(3)} \le z \le 0, y = \pm\beta)$.

The present study proceeds under the assumptions that the fluid is inviscid and incompressible, and the motion is irrotational and simple harmonic in time with angular frequency ω. These assumptions ensure that the velocity potential $\Phi(x,y,z,t)$ exists which can be written as $\Phi(x,y,z,t) = \mathrm{Re}[\phi(x,y,z)e^{-i\omega t}]$, Re being the real part. In the fluid domain, the spatial velocity potential $\phi(x,y,z)$ satisfies the three dimensional Laplace equation

$$\nabla^2\phi(x,y,z) = 0. \tag{1}$$

It is subjected to the linearized free surface boundary condition

$$\partial_z\phi - (\omega^2/g)\phi = 0, \text{ on } z = 0, \tag{2}$$

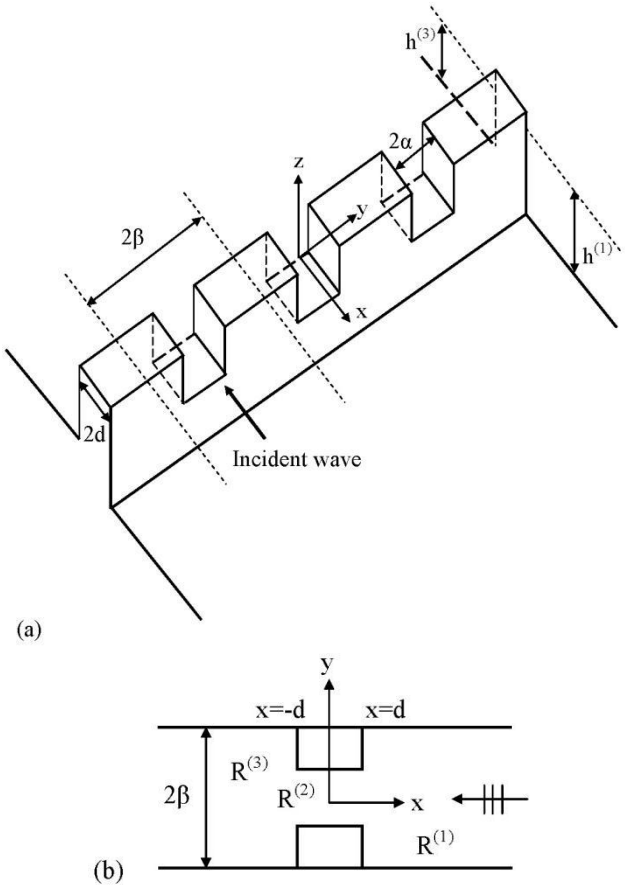

Fig. 1 (a) Schematic view of array of breakwaters and (b) top view of channel problem

along with the no-flux boundary condition on the surfaces of sea bed (S_b), breakwater (S_{bw}) and channel walls (S_{cw}), which is defined by

$$\partial_n \phi = 0, \quad \text{on } S_b, S_{bw}, \text{ and } S_{cw}, \tag{3}$$

where g is the gravitational constant and n represents the outward normal on the surfaces. In addition, the far-field radiation condition is given by

$$\lim_{r\to\pm\infty} \sqrt{r}\left(\frac{\partial}{\partial r} - ik^{(j)}\right)\phi = 0, \tag{4}$$

where $r = \sqrt{x^2+y^2}$, and j = 1 and 3 are associated with ∞ and -∞, respectively. Further, $k^{(1)}$ and $k^{(3)}$ indicate the incident and reflected wave numbers in the domains $R^{(1)}$ and $R^{(3)}$, respectively.

The velocity potentials $\phi^{(j)}$ for different domains $R^{(j)}$, j = 1, 2 and 3, can be derived from the above boundary value problem using the eigenfunction expansion method. Solving the governing Eq. (1) along with the boundary conditions (2) - (4) (see Mondal *et al.* 2017), the velocity potentials for each domain can be expanded as

$$\begin{aligned}\phi^{(j)} = &\left\{\delta_{1j} I e^{-ik_0^{(j)}(x-d)} f_0^{(j)}(z) + \sum_{n=0}^{\infty} A_{0n}^{(j)} e^{\pm ik_n^{(j)}(x\mp d)} f_n^{(j)}(z)\right\} \\ &+ \sum_{m=1}^{\infty} \cos\lambda_m(\beta - y) \sum_{n=0}^{\infty} A_{mn}^{(j)} e^{\pm ip_{mn}^{(j)}(x\mp d)} f_n^{(j)}(z), \quad \text{for j=1, 3,}\end{aligned} \tag{5}$$

and

$$\begin{aligned}\phi^{(2)} = &\sum_{n=0}^{\infty}\left\{A_{0n}^{(2)}\frac{\cos k_n^{(2)}x}{\cos k_n^{(2)}d} + B_{0n}^{(2)}\frac{\sin k_n^{(2)}x}{\sin k_n^{(2)}d}\right\} f_n^{(2)}(z) \\ &+ \sum_{m=1}^{\infty}\cos\gamma_m(\alpha - y)\sum_{n=0}^{\infty}\left\{A_{mn}^{(2)}\frac{\cos p_{mn}^{(2)}x}{\cos p_{mn}^{(2)}d} + B_{mn}^{(2)}\frac{\sin p_{mn}^{(2)}x}{\sin p_{mn}^{(2)}d}\right\} f_n^{(2)}(z),\end{aligned} \tag{6}$$

where δ_{1j} is the Kronecker delta and the eigenvalues $k_n^{(j)}$, j = 1, 2 and 3 satisfy the dispersion relation in $k^{(j)}$ given by

$$\omega^2 = gk^{(j)}\tanh k^{(j)}h^{(j)}, \tag{7}$$

which has one positive real root $k_0^{(j)}$ and an infinite number of imaginary roots $ik_n^{(j)}$. The parameters λ_m, γ_m and $p_{mn}^{(j)}$ are given by

$$\lambda_m = \frac{m\pi}{\beta},\ \gamma_m = \frac{m\pi}{\alpha},\ p_{mn}^{(j)} = \sqrt{(k_n^{(j)})^2 - \lambda_m^2},\ j = 1,3, \text{ and } p_{mn}^{(2)} = \sqrt{(k_n^{(2)})^2 - \gamma_m^2}, \tag{8}$$

for m = 1, 2,... and n = 0, 1, 2,.... The eigenfunctions $f_n^{(j)}(z)$, j = 1, 2 and 3 as appearing in Eqs. (5) and (6) are of the form

$$f_n^{(j)}(z) = \frac{\cosh k_n^{(j)}\left(h^{(j)} + z\right)}{\cosh k_n^{(j)}h^{(j)}}, \quad \text{for n = 0, 1, 2,…,} \tag{9}$$

which satisfy the orthogonal relation

$$\left\langle f_n^{(j)}(z), f_v^{(j)}(z)\right\rangle = \int_{-h^{(j)}}^{0} f_n^{(j)}(z) f_v^{(j)}(z)dz = \mathcal{D}_v^{(j)}\delta_{nv}, \tag{10}$$

where δ_{nv} is the Kronecker delta, and the orthogonality constants $\mathcal{D}_v^{(j)}$ is of the form

$$\mathcal{D}_v^{(j)} = \frac{2k_v^{(j)}h^{(j)} + \sinh 2k_v^{(j)}h^{(j)}}{4k_v^{(j)}\cosh^2 k_v^{(j)}h^{(j)}}, \quad \text{for v = 0, 1, 2,…} \tag{11}$$

The sequence $\{\cos\gamma_m(\alpha - y), m = 0,1,2,...\}$ is orthogonal over 2α, and the orthogonality relation is defined by

$$\int_{-\alpha}^{\alpha}\cos\gamma_m(\alpha - y)\cos\gamma_u(\alpha - y)dy = \varepsilon\alpha\delta_{mu} \tag{12}$$

where ε = 2 for u = 0, otherwise unity, and δ_{mu} represents the Kronecker delta. Further, the sequence $\{\cos\lambda_m(\beta - y), m = 0,1,2,...\}$ also satisfies the same relation as defined in Eq. (12) in the interval -β ≤ y ≤ β.

In Eq. (5), I is a known quantity associated with the incident wave height. Furthermore, the coefficients $A_{00}^{(1)}$ and $A_{00}^{(3)}$ are related with reflected and transmitted wave heights in domains $R^{(1)}$ and $R^{(3)}$, respectively. Lastly, it is required to find out the unknown complex constants $A_{mn}^{(j)}$ (j = 1,2,3), and $B_{mn}^{(2)}$ (m = 1,2,..., n = 0,1,2,...) to know the velocity potentials completely. The unknowns can be determined by using the matching of velocity and pressure as defined by

$$\phi^{(j)} = \phi^{(j+1)} \text{ and } \partial_x\phi^{(j)} = \partial_x\phi^{(j+1)}, \text{ for } j = 1,2 \text{ and } -\alpha \le y \le \alpha, -h^{(2)} \le z \le 0, \tag{13}$$

at the interfaces x = ±d and the relations as in Eqs. (3), (10) and (12). Proceeding in a similar manner as in Mondal *et al.* (2017), a system of linear algebraic equations is obtained as follows

$$\sum_{n=0}^{\infty} 2\alpha X_{nv}^{(j)}A_{0n}^{(j)} + \sum_{m=1}^{\infty} J_{m0}\sum_{n=0}^{\infty} X_{nv}^{(j)}A_{mn}^{(j)} - 2\alpha\mathcal{D}_v^{(2)}\left[A_{0v}^{(2)} \pm B_{0v}^{(2)}\right] = -2\alpha I X_{0v}^{(j)}\delta_{1j}, \tag{14a}$$

$$\sum_{m=1}^{\infty} J_{mu}\sum_{n=0}^{\infty} X_{nv}^{(j)}A_{mn}^{(j)} - \alpha\mathcal{D}_v^{(2)}\left[A_{uv}^{(2)} \pm B_{uv}^{(2)}\right] = 0, \text{ for } u = 1,2,..., \tag{14b}$$

$$2i\beta k_v^{(j)}\mathcal{D}_v^{(j)}A_{0v}^{(j)} + 2\alpha\sum_{n=0}^{\infty} k_n^{(2)}X_{vn}^{(j)}\left[A_{0n}^{(2)}\tan k_n^{(2)}d \mp B_{0n}^{(2)}\cot k_n^{(2)}d\right] = 2i\beta I k_v^{(j)}\mathcal{D}_v^{(j)}\delta_{1j}\delta_{v0}, \tag{15a}$$

$$\begin{aligned}&ip_{uv}^{(j)}\beta\mathcal{D}_v^{(j)}A_{uv}^{(j)} + \sum_{n=0}^{\infty} k_n^{(2)}\left[A_{0n}^{(2)}\tan k_n^{(2)}d \mp B_{0n}^{(2)}\cot k_n^{(2)}d\right]X_{vn}^{(j)}J_{u0} \\ &\quad + \sum_{m=1}^{\infty}\sum_{n=0}^{\infty} q_{mn}\left[A_{mn}^{(2)}\tan p_{mn}^{(2)}d \mp B_{mn}^{(2)}\cot p_{mn}^{(2)}d\right]X_{vn}^{(j)}J_{um} = 0, \quad u = 1,2,...,\end{aligned} \tag{15b}$$

for v = 0, 1, 2, ... and j = 1, 3. The sign '+' and '-' in Eq. (14) correspond to j = 1 and j = 3, respectively whereas in Eq. (15) the sign '+' and '-' correspond to j = 3 and j = 1, respectively. The integrals $X_{nv}^{(j)}$, (n, v = 0, 1, 2, ...,) and J_{mu}, (m = 1, 2, ..., u = 0, 1, 2, ...) are of the forms

$$X_{nv}^{(j)} = \frac{1}{\left(k_v^{(2)}\right)^2 - \left(k_v^{(j)}\right)^2}\left[k_v^{(2)}\tanh k_v^{(2)}h^{(2)} - k_n^{(2)}\left\{\tanh k_n^{(j)}h^{(j)} - \frac{\sinh k_n^{(j)}\left(h^{(j)} - h^{(2)}\right)}{\cosh k_n^{(j)}h^{(j)}\cosh k_v^{(2)}h^{(2)}}\right\}\right] \tag{16}$$

$$J_{mu} = \int_{-\alpha}^{\alpha}\cos\lambda_m(\beta - y)\cos\gamma_u(\alpha - y)dy = \frac{2(-1)^m\lambda_m\sin\lambda_m\alpha}{\lambda_m^2 - \gamma_u^2}. \tag{17}$$

The integrals $X_{vn}^{(j)}$ and J_{um} as appear in Eqs. (15(a)) and (15(b)) can be obtained from Eqs. (16) and (17), respectively, by interchanging the suffix (n, v) and (m, u).

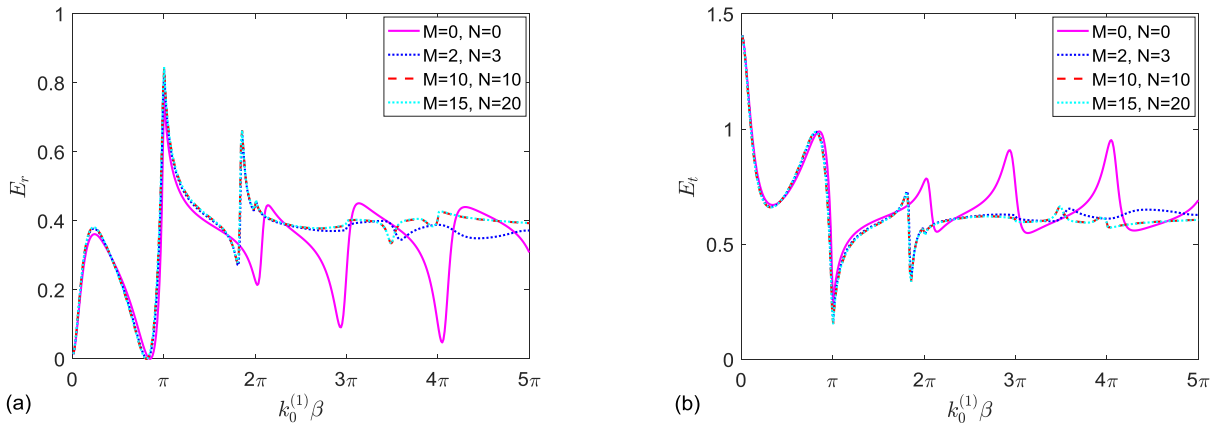

Fig. 2 (a) E_r and (b) E_t versus non-dimensional wavenumber $k_0^{(1)}\beta$ for different values of M and N

The constants $A_{mn}^{(j)}$ (j = 1, 2, and 3) and $B_{mn}^{(2)}$ can be evaluated by solving the system of algebraic Eqs. (14) and (15). It is observed that the series are infinite over m and n. Thus, for numerical computation, it is required to consider finite values of m and n. The series over m and n are truncated for $m = M$ and $n = N$ leading $4(M + 1)(N + 1)$ unknowns. The computation of unknowns will lead to finding out the physical quantities: reflected, transmitted wave energy and wave field in the vicinity of breakwaters.

3. Results and discussion

The derived velocity potential in Eq. (5) depicts that a progressive wave train exists in domains $R^{(1)}$ and $R^{(3)}$ and propagates along the x-axis. Further, in domains $R^{(1)}$ and $R^{(3)}$, a group of oblique waves exist when $k_0^{(1)}\beta > \pi$ and $k_0^{(3)}\beta > \pi$, respectively. These oblique waves exist in pair and intersect the x-axis making an angle $\pm\cos^{-1}\sqrt{\left(k_0^{(j)}\right)^2 - \lambda_m^2}\,/\,k_0^{(j)}$ with the x-axis (Dalrymple and Martin 1990, Williams and Crull 1993, Mondal *et al.* 2017) where j= 1 and 3 indicate domains $R^{(1)}$ and $R^{(3)}$, respectively. Hence, the wave energy is carried out by the plane waves propagating along the x-axis and oblique waves. Therefore, considering the energy flux in domains $R^{(1)}$ and $R^{(3)}$, the energy identity can be written as (see Mondal and Alam 2018)

$$E_r + \kappa E_t = 1, \tag{18}$$

where $\kappa = \mathcal{D}_0^{(3)} / \mathcal{D}_0^{(1)}$. The total reflected energy (E_r) in domain $R^{(1)}$ and transmitted energy (E_t) in domain $R^{(3)}$ are given by

$$E_r = K_{r0}^2 + \sum_{m=1}^{M_1} \frac{p_{m0}^{(1)}}{2k_0^{(1)}} K_{rm}^2, \quad \text{and} \quad E_t = \frac{k_0^{(3)}}{k_0^{(1)}} K_{t0}^2 + \sum_{m=1}^{M_2} \frac{p_{m0}^{(3)}}{2k_0^{(1)}} K_{tm}^2. \tag{19}$$

The m-th mode of reflection coefficient (K_{rm}) and transmission coefficient (K_{tm}) are given by $K_{rm} = |A_{m0}^{(1)} / I|$ and $K_{tm} = |A_{m0}^{(3)} / I|$ where M_1 and M_2 indicate the number of oblique waves in domains $R^{(1)}$ and $R^{(3)}$, respectively.

For numerical computation, the values of different physical parameters are considered as $h^{(2)}/h^{(1)}$ = 0.4, $h^{(3)}/h^{(1)}$ = 0.7, α/β = 0.6 and d/β = 0.4 unless it is mentioned. The non-dimensional surface deflection is defined by $\bar{\eta}^{(j)} = i\bar{\omega}\bar{\phi}^{(j)}$, for j = 1, 2, and 3, where $\bar{\phi}^{(j)} = \phi^{(j)} / (I\sqrt{\beta g})$.

In section 2, we have mentioned that the infinite series are truncated for $m = M$ and $n = N$. Thus, we need to find out the minimum values of M and N for which the numerical results converge. To examine the convergence of infinite series (Eqs. (5) and (6)) numerically in Fig. 2, we have plotted total reflected energy (E_r) and transmitted energy (E_t) against non-dimensional wave number $k_0^{(1)}\beta$ for different values of M and N. Fig. 2 depicts that the values of (E_r) and (E_t) are approximately the same for (M = 10, N = 10) and (M = 15, N = 20) in the range $0.01 < k_0^1\beta < 5\pi$. Hence, it is sufficient to consider (M = 10, N = 10) for the numerical computation.

The energy relation defined in Eq. (18) is compared with numerical values of $E_r + \kappa E_t$ (Table 1) for different values of $k_0^{(1)}\beta$ (= $\pi/4$, $2\pi/3$, $3\pi/2$, $5\pi/2$, $7\pi/2$, and $9\pi/2$). In addition, in Table 1, values of absolute percentage error (e_r) are presented. It is observed that the maximum value of the absolute percentage error is 10^{-4}. This confirms that computed results are accurate.

Before proceeding further, in order to confirm the accuracy of the present method, we have compared our results with the known numerical results of Dalrymple and Martin (1990) who considered screen type inline breakwaters with a uniform water depth. From the formulation of the present problem, it is obvious that for the numerical computation we can not equate d/β with zero, and $h^{(2)}/h^{(1)}$ and $h^{(3)}/h^{(1)}$ with unity. Hence, in Fig. 3, we have plotted the zeroth order reflection coefficient K_{r0} and phase $-\theta/\pi$ versus non-dimensional wavenumber $k_0^{(1)}\beta$ for

Table 1 Numerical check of energy relation (18) for different values of $k_0\beta$

$k_0^{(1)}\beta$	R_{total}	T_{total}	κ	$R_{total}+\kappa T_{total}$	e_r
π/4	0.380206	0.682971	0.907497	1.00000013	0.000013
2π/3	0.106118	0.871601	1.025564	1.00000061	0.000061
3π/2	0.411313	0.588606	1.000136	0.99999905	0.000095
5π/2	0.382275	0.617725	1.000001	1.000001	0.000062
7π/2	0.337541	0.662458	1	0.99999936	0.000064
9π/2	0.403261	0.596738	1	0.999999	0.0001

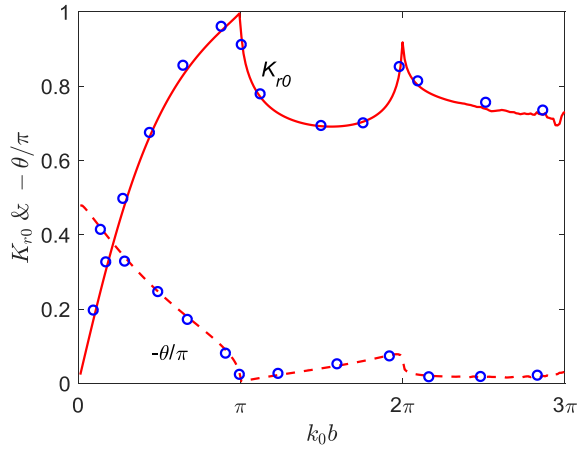

Fig. 3 Comparison of present result (lines) with Dalrymple and Martin's (1990) (symbols)

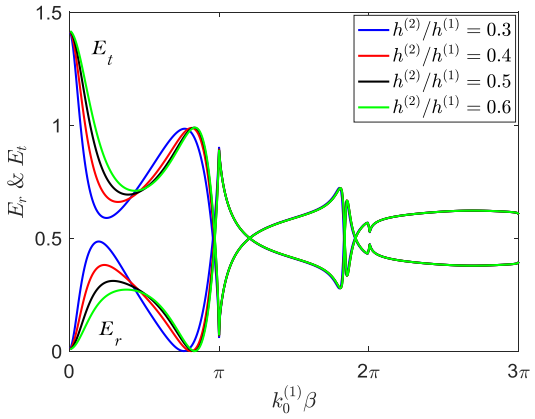

Fig. 5 Total reflected and transmitted wave energy versus non-dimensional wavenumber $k_0^{(1)}\beta$ for different depth ration $h^{(2)}/h^{(1)}$ with α/β = 0.6, d/β = 0.4 and $h^{(3)}/h^{(1)}$ = 0.7

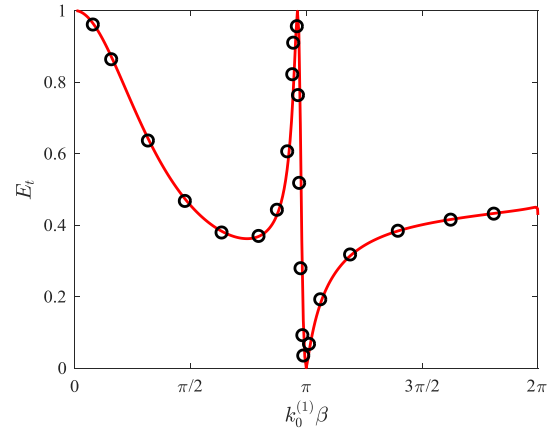

Fig. 4 Total transmitted energy (E_t) versus non-dimensional wavenumber $k_0^{(1)}\beta$. The line and circles indicate present results and Fernyhough and Evans' (1995)

d/β = 0.0001, α/β = 0.25 $h^{(2)}/h^{(1)}$ = 0.9998, and $h^{(3)}/h^{(1)}$ = 0.9999, where the amplitude and phase are defined by K_{r0} = $|K_{r0}|e^{i\theta}$ (Dalrymple and Martin 1990). In the figure circle symbols indicate the results of Dalrymple and Martin (1990). Both results agree well with each other.

In Fig. 4, another comparison of the present result is made with the result of Fernyhough and Evans (1995) who considered a periodic array of rectangular breakwaters and uniform water depth. As stated before, we can not substitute $h^{(2)}/h^{(1)}$ = 1 and $h^{(3)}/h^{(1)}$ = 1. Therefore, we consider sufficiently close values of $h^{(2)}/h^{(1)}$ = 0.9998 and $h^{(3)}/h^{(1)}$ = 0.9999 and plotted the total transmitted energy E_t as a function of $k_0^{(1)}\beta$ with α/β = 0.4 and d/β = 0.2. From Fig. 4, we can see that the present results (line) have a good agreement with the result (circular symbols) of Fernyhough and Evans (1995).

3.1. Effect of $h^{(2)}/h^{(1)}$

Variations of reflected wave energy (E_r) and transmitted wave energy (E_t) with $k_0^{(1)}\beta$ are presented in Fig. 5 for different values of $h^{(2)}/h^{(1)}$ (= 0.3, 0.4, 0.5, and 0.6) with d/β = 0.4. It is noticed that, with an increase in $k_0^{(1)}\beta$, the E_r grows and E_t declines, attaining a maximum and a minimum, respectively for certain values of $k_0^{(1)}\beta$ (< π/2). After the maximum and minimum values, E_r decreases to zero and E_t becomes unity accordingly for $k_0^{(1)}\beta$ = 0.76π − 0.83π depending on $h^{(2)}/h^{(1)}$. It is also observed that there is

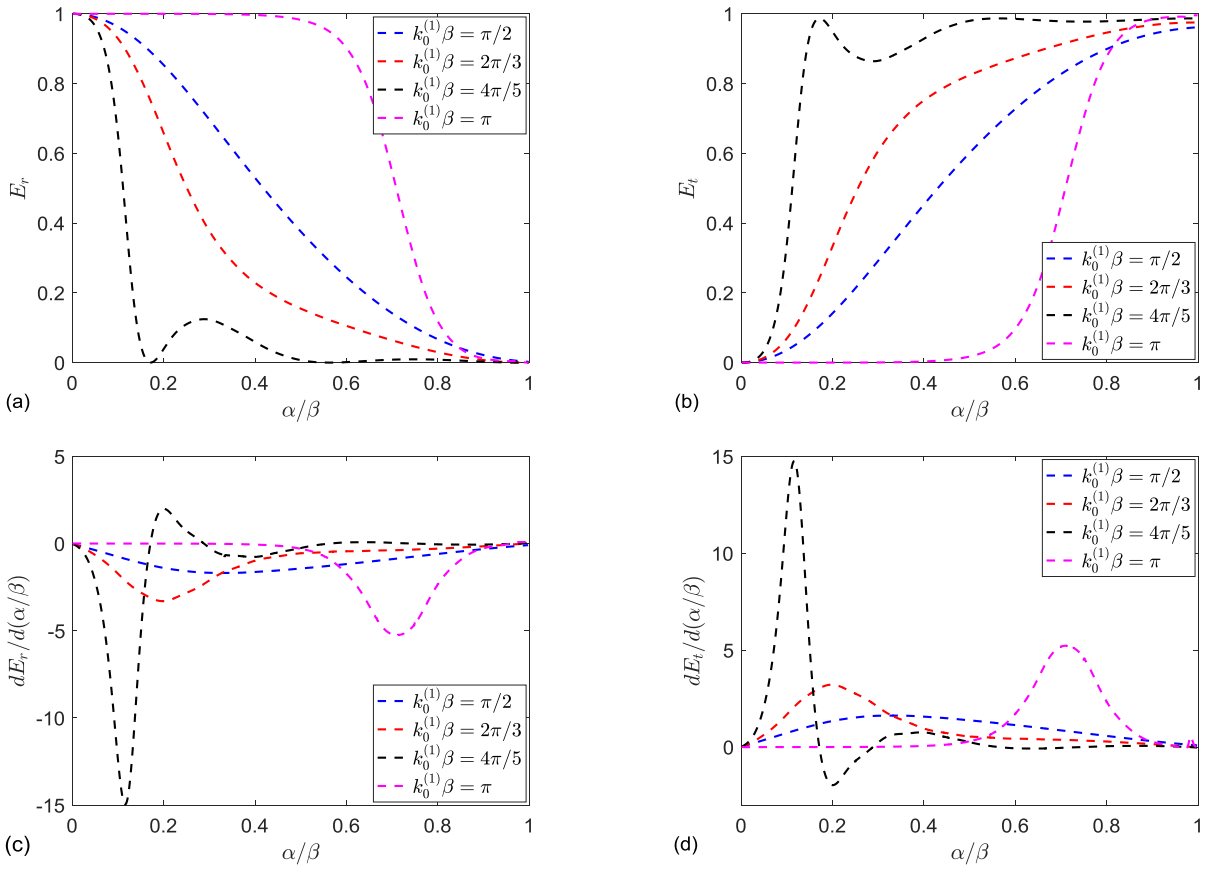

Fig. 6 (a) Reflected energy and (b) transmitted energy versus α/β for different wave number $k_0^{(1)}\beta$ with $d/\beta = 0.4$, $h^{(2)}/h^{(1)} = 0.4$ and $h^{(3)}/h^{(1)} = 0.7$

no change in the values of E_r and E_t with the change of $h^{(2)}/h^{(1)}$ for $k_0^{(1)}\beta > \pi$. Furthermore, from Fig. 5, it is seen that there are sharp changes in E_r and E_t at $k_0^{(1)}\beta = m\pi$, where m = 1, 2, ... This happens as the channel width becomes an integer multiple of the wavelength which indicates that the cross tank modes are excited.

3.2 Effect of α/β

The variations of E_r and E_t with the gap ratio (α/β) of the gap length (α) and channel width (β) are plotted in Fig. 6(a) and 6(b) for different values of $k_0^{(1)}\beta$ (= π/2, 2π/3, 4π/5, and π). For a given $k_0^{(1)}\beta$, the E_r and E_t vary oppositely to each other with the increase of α/β. The E_r is 1.0 at α/β ≈ 0 regardless of $k_0^{(1)}\beta$, i.e., the energy is totally reflected, yielding E_t = 0. On the other hand, when α/β = 1.0, the energy is totally transmitted (E_t = 1.0) as expected. The E_r for $k_0^{(1)}\beta = \pi/2$ decreases with increasing α/β, having an inflection point at α/β = 0.33 (Fig. 6(c)) where E_r = 0.64. It suggests that the rate of the decrease grows for α/β < 0.33 and declines for α/β > 0.33 (Fig. 6(c)). When $k_0^{(1)}\beta$ is increased to 2π/3, the inflection point shifts forward, occurring at α/β = 0.20 with E_r = 0.66. That is, the E_r declines more rapidly for α/β < 0.20 with more energy transmitted (Figs. 6(c) and 6(d)). A further increase in $k_0^{(1)}\beta$ to 4π/5 produces interesting results, E_r sharply dropping to zero at α/β = 0.17, followed by an increase upto α/β = 0.29. In other words, the energy is totally transmitted at α/β = 0.17. An inflection point again exists at α/β = 0.12 where E_r = 0.44. At $k_0^{(1)}\beta = \pi$, the $E_r \approx 1.0$ for α/β < 0.5, decaying for α/β > 0.5. The observation suggests that the energy is not transmitted at all for $k_0^{(1)}\beta = \pi$ when α/β < 0.5. Here the inflection point occurs at α/β = 0.71 with E_r = 0.49. These α/β corresponding to the inflection points can be called as the critical $(\alpha/\beta)_i$ which render some important realities that a change in α/β upto $(\alpha/\beta)_i$ allows energy transmission at a greater rate and about 1/3 of the total energy is transmitted to the lee side for most of the cases. One question may arise what is the insight into the relationship between $(\alpha/\beta)_i$ and $k_0^{(1)}\beta$. As found above, $(\alpha/\beta)_i$ = 0.33, 0.2, 0.12 and 0.71 for $k_0^{(1)}\beta = \pi/2, 2\pi/3, 4\pi/5$, and π, respectively. The $k_0^{(1)}\beta = 2\pi/3$, for example, means that a length of β contains 2/3 of the wave. The $k_0^{(1)}\beta = m\pi = (k_0^{(1)}\beta)_0$ represents an integer number of waves lying on β, where m = 1, 2, ... So, $((k_0^{(1)}\beta)_0 - k_0^{(1)}\beta)$ is the deficit

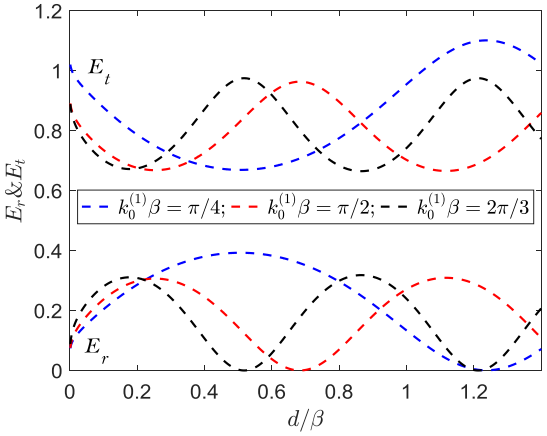

Fig. 7 Total reflected and transmitted wave energy versus d/β for different wave number $k_0^{(1)}\beta$ with $\alpha/\beta = 0.6$, $h^{(2)}/h^{(1)} = 0.4$ and $h^{(3)}/h^{(1)} = 0.7$

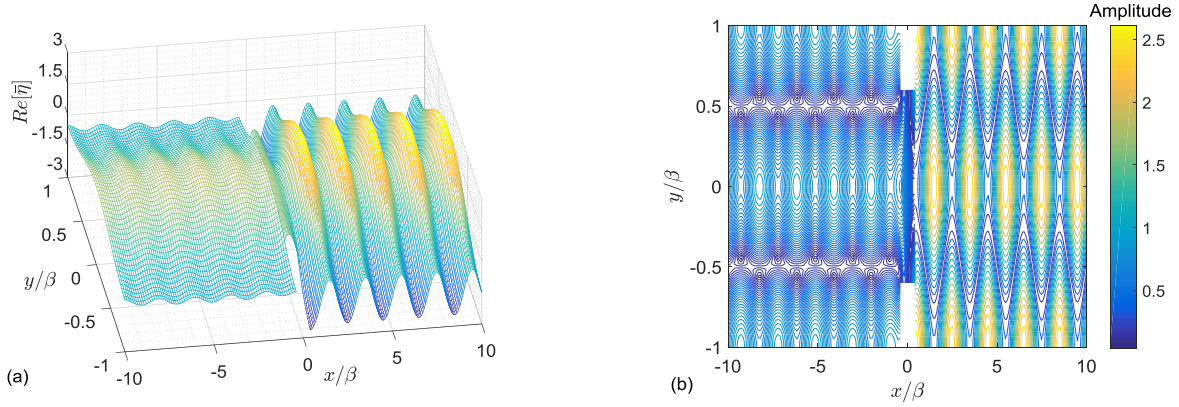

Fig. 8 Real part of surface elevation and (b) flow distribution in the vicinity of breakwaters with $\alpha/\beta = 0.6$, $d/\beta = 0.4$ and $k_0^{(1)}\beta = \pi$.

wavenumber. Interestingly, we find that $(\alpha/\beta)_i / \left(\left(k_0^{(1)}\beta\right)_0 - k_0^{(1)}\beta\right)$ = 0.66/π, 0.6/π, 0.6/π, and 0.71/π, respectively, which can be roughly represented by ~ 2/3π. Note that m = 2 for $k_0^{(1)}\beta = \pi$ as $\left(k_0^{(1)}\beta\right)_0 - k_0^{(1)}\beta > 0$. The factor $(\alpha/\beta)_i / \left(\left(k_0^{(1)}\beta\right)_0 - k_0^{(1)}\beta\right)$ can be regarded as the non-dimensional opening of the channel considering both β and $k_0^{(1)}$. This information may be very useful for the breakwater designers.

3.3 Effect of d/β

Reflected wave energy E_r and transmitted wave energy E_t are plotted in Fig. 7 as a function of d/β for different values of $k_0^{(1)}\beta$. It is noticed that the variations in E_r and E_t with d/β for each $k_0^{(1)}\beta$ are periodic. For $k_0^{(1)}\beta = \pi/4$, E_t becomes minimum at $d/\beta = 0.5$, i.e., for waves of a large wavelength, the breakwater width should be half of the channel width for a minimum transmission of energy. On the other hand, the corresponding values of d/β for a minimum E_t are 0.26 and 0.18 for $k_0^{(1)}\beta = \pi/2$ and $2\pi/3$, respectively. The observation suggests that, for a minimum E_t, a smaller thickness of breakwaters is required for waves of a smaller wavelength. The value of d/β, at which E_t attains a minimum, is called critical $(d/\beta)_c$. Further, it is noticed that $(d/\beta)_c \times k_0^{(1)}\beta \approx \pi/8$. That is, when a minimum E_t is required, one can calculate the required d from this empirical relation.

Wave fields in the vicinity of breakwaters are presented in Figs. 8-10. The incident wave trains arrive from the right sides of the figures. In Fig. 8, the real part of the surface profile and modulus of the wave field are plotted for $k_0^{(1)}\beta = \pi$, i.e the wavelength is equal to the channel width 2β. Hence, a cross-tank wave mode is observed in domains $R^{(1)}$ and $R^{(3)}$. It is apparent that the free surface mode in domains $R^{(1)}$ and $R^{(3)}$ has a cosine mode in the lateral direction as expected. For a large $d/\beta = 2.0$ and $k_0^{(1)}\beta = 7\pi/4$, the surface profile, surface elevation along the x-axis and flow distribution are plotted in Fig. 9. In this

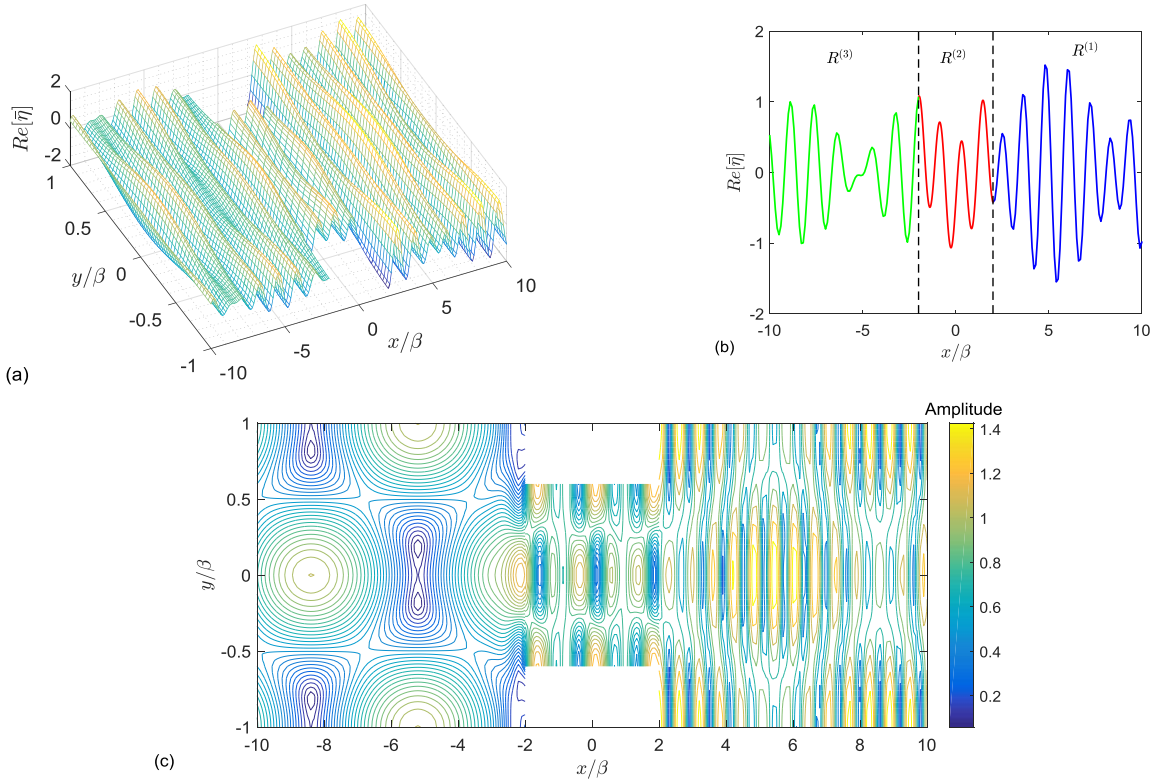

Fig. 9 (a) Real part of surface elevation, (b) surface elevation along the *x*-axis, and (c) flow distribution in the vicinity of breakwaters with α/β = 0.6, *d*/β = 2.0 and $k_0^{(1)}\beta = 7\pi/4$

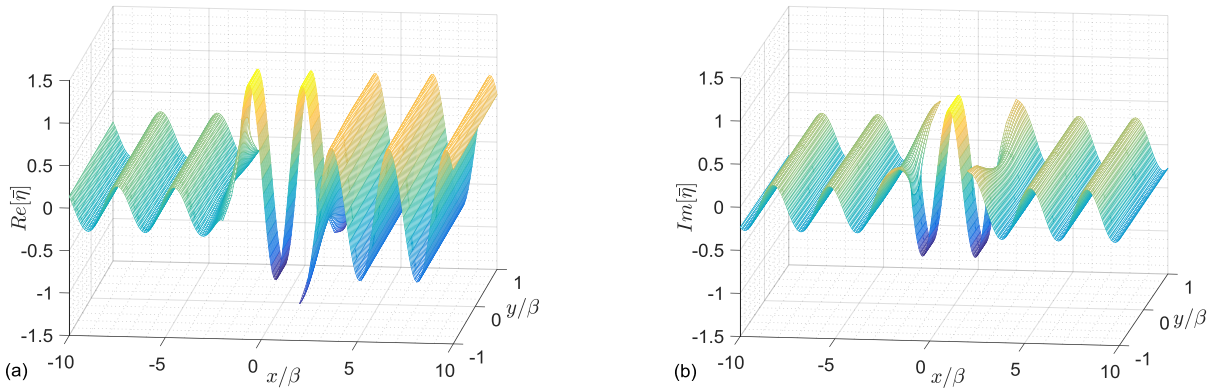

Fig. 10 Free surface deformation (a) real part and (b) imaginary part with α/β = 0.2, *d*/β = 2.0 and $k_0^{(1)}\beta = 2\pi/3$

case, the wave field consists of a progressive wave along the *x*-axis and a pair of oblique waves. Using the expression $\pm\cos^{-1}\sqrt{\left(k_0^{(1)}\right)^2 - \lambda_m^2}\,/\,k_0^{(1)}$, it is found that the pair of oblique waves intersect the *x*-axis at angles 35^o and 145^o with the positive direction of the *x*-axis. Hence the wave field becomes more complicated in this case. Further, in the ocean side, partial standing waves are observed in front of the breakwater mouth, while the progressive wave is observed on the lee side. From Figs. 8(b) and 9(c), it is obvious that the wave amplitude on the lee side of breakwaters is smaller than that on the ocean side.

In Fig. 10, real part and imaginary part of surface elevation are plotted for $k_0^{(1)}\beta = 2\pi/3$ where α/β = 0.2 and *d*/β = 2.0. However, the water depth is considered the same as stated above. In sea side, the surface profile for real and imaginary parts are of 90^o phase lag and the amplitudes are not equal. This implies that partial standing wave is formed in sea side. On the other hand, the progressive wave is observed in the lee side of breakwaters.

4. Conclusions

In this study, we have considered the problem of wave interaction with a group of identical rectangular structures in the presence of undulated bottom topography. The problem is converted into a boundary value problem in terms of velocity potential and solved by using the eigenfunction expansion method. Using the matching conditions at interfaces of two different domains, a system of linear algebraic equations are constructed and solved numerically using commercial software MATLAB to know the velocity potentials completely.

From the numerical computation, it is observed that the present method has a good agreement with the results in the literature. We have presented the reflected and transmitted energy for different physical parameters, along with the wave field in the vicinity of breakwaters. At $k_0\beta = \pi$, where the wavelength becomes equal to the channel width, sharp changes in the reflected and transmitted energy are observed, E_t dropping to ≈ 0 and E_r jumping to ≈ 1, because of an occurrence of a cross-tank resonance mode. In the case of small wavelength (< 2β), a pair of oblique waves appear along with the travelling wave along the *x*-axis and the wave pattern becomes more complicated. Furthermore, the surface profiles, suggests that the breakwaters are efficient to provide a relatively calm zone in the lee side. For each $k_0^{(1)}\beta$, there is a critical $(\alpha/\beta)_i$ following $(\alpha/\beta)_i / \left(\left(k_0^{(1)}\beta\right)_0 - k_0^{(1)}\beta\right) = 2/3\pi$ that corresponds to 1/3 of the total energy transmitted to the lee side. On the other hand, it is observed that, for the minimum transmission of wave energy, the width of breakwaters is linearly proportional to the wavelength which follows $(d/\beta)_c \times k_0^{(1)}\beta \approx \pi/8$. The reflected and transmitted wave energy does not vary with $h^{(2)}/h^{(1)}$ when the wavelength is smaller than the channel width (i.e., $k_0^{(1)}\beta < \pi$).

Acknowledgments

The authors wish to acknowledge the support given to them from National Nature Science Foundation of China through grants 11672096 and 91752112 and from Research Grant Council of Shenzhen Government through grants JCYJ20170811152808282 and JCYJ20180306171921088.

References

Abul-Azm, A.G. and Williams, A.N. (1997), "Oblique wave diffraction by segmented offshore breakwaters", *Ocean Eng.*, **24**(1), 63-82. https://doi.org/10.1016/0029-8018(95)00065-8.

Achenbach, J.D. and Li, Z.W. (1986), "Reflection and transmission of scalar waves by a periodic array of screens", *Wave Motion*, **8**(3), 225-234. https://doi.org/10.1016/S0165-2125(86)80045-2.

Belibassakis, K.A., Tsoukala, V.K. and Katsardi, V. (2014), "Three-dimensional wave diffraction in the vicinity of openings in coastal structures", *Appl. Ocean Res.*, **45**, 40-54. https://doi.org/10.1016/j.apor.2013.12.005.

Bhattacharjee, J., Karmakar, D. and Sahoo, T. (2008), "Transformation of flexural gravity waves by heterogeneous boundaries", *J. Eng. Math.*, **62**(2), 173-188.

Buchwald, V.T. (1971), "The diffraction of tides by a narrow channel", *J. Fluid Mech.*, **46**(3), 501-511. https://doi.org/10.1017/S0022112071000661.

Dalrymple, R.A. and Martin, P.A. (1990), "Wave diffraction through offshore breakwaters", *J. Waterway, Port, Coastal, Ocean Eng.*, **116**(6), 727-741. https://doi.org/10.1061/(ASCE)0733-950X(1990)116:6(727).

Dalrymple, R.A., Martin, P.A. and Li, L. (2000), "Waves in rectangular inlet with reflecting or absorbing walls", *J. Waterway, Port, Coastal, Ocean Eng.*, **126**(6), 288-296. https://doi.org/10.1061/(ASCE)0733-950X(2000)126:6(288).

Dhillon, H., Banerjea, S. and Mandal, B.N. (2016), "Water wave scattering by a finite dock over a step type bottom topography", *Ocean Eng.*, **113**, 1-10. https://doi.org/10.1016/j.oceaneng.2015.12.017.

Fernyhough, M. and Evans, D.V. (1995), "Scattering by a periodic array of rectangular blocks", *J. Fluid Mech.*, **305**, 263-279. https://doi.org/10.1017/S0022112095004629.

Kanoria, M., Dolai, D.P. and Mandal, B.N. (2014), "Water-wave scattering by thick vertical barriers", *J. Eng. Math.*, **35**(4), 361-384.

Karmakar, D. and Sahoo, T. (2008), "Gravity wave interaction with floating membrane due to abrupt change in water depth", *Ocean Eng.*, **35**(7), 598-615. https://doi.org/10.1016/j.oceaneng.2008.01.009.

Linton, C.M. and Evans, D.V. (1993), "Acoustic scattering by an array of parallel plates", *Wave Motion*, **18**(1), 51-65. https://doi.org/10.1016/0165-2125(93)90060-S.

Miles, J.W. (1982), "On Rayleigh scattering by a gratting", *Wave Motion*, **2**, 285-292.

Mondal, R. and Alam, M.M. (2018), "Water wave scattering by an array of rectangular breakwaters on step bottom topography", *Ocean Eng*, **169**, 359-369. https://doi.org/10.1016/j.oceaneng.2018.09.039.

Mondal, R., Takagi, K. and Wada, R. (2017), "Diffraction problem of a floating breakwater with an array of small ports", *J. Mar. Sci. Technol.*, **22**(3), 459-469.

Mondal, R. and Takagi, K. (2017), "Wave scattering by a fixed submerged platform over a step bottom", *Proc. IMechE. Part M: J. Eng. Mari. Envi.*, **233**(1), 93-107. https://doi.org/10.1177/1475090217718922.

Newman, J.N. (1965), "Propagation of water waves over an infinite step", *J. Fluid Mech.*, **23**(2), 399-415. https://doi.org/10.1017/S0022112065001453.

Porter, R. and Evans, D.V. (1996), "Wave scattering by periodic arrays of breakwaters", *Wave Motion*, **23**(2), 95-120. https://doi.org/10.1016/0165-2125(95)00049-6.

Sobey, R.J. and Johnson, T.L. (1986), "Diffraction patterns near narrow breakwater gaps", *J. Waterway, Port, Coastal, Ocean Eng.*, **112**(4), 512-528. https://doi.org/10.1061/(ASCE)0733-950X(1986)112:4(512).

Tsoukala, V.K. and Moutzouris, C.I. (2009), "Wave transmission in harbors through flushing culverts", *Ocean Eng.*, **36**(6-7), 434-445. https://doi.org/10.1016/j.oceaneng.2009.01.005.

Williams, A.N. and Crull, W.W. (1993), "Wave diffraction by array of thin-screen breakwaters", *J. Waterway, Port, Coastal, Ocean Eng.*, **119**(6), 606-617. https://doi.org/10.1061/(ASCE)0733-950X(1993)119:6(606).